Contributions to absorption line weakening in the Earth's atmosphere

Kyle Penner and Carlos Allende Prieto

Department of Astronomy, University of Texas at Austin
1 University Station C1400, Austin, TX 78712-0259

kpenner@mail.utexas.edu

ABSTRACT

Daytime skylight is an imperfect representation of the solar spectrum. Scattering of light in the Earth's atmosphere changes the depths of solar absorption lines. This scattering is due to either molecules or dust grains in the Earth's atmosphere. Additionally, ground-albedo, the reflection of sunlight from the Earth's surface back into the atmosphere, may play an important role in diluting the strength of absorption lines. The relative importance of each process is not understood – some studies suggest that ground-albedo is not important, while others indicate that it is significant. We examine the filling-in of absorption lines as a function of angular separation from the Sun, replicating previous measurements with a much richer dataset; because we have line data for the Sun's entire optical spectrum, we more clearly determine what processes are important.

1. Introduction

Absorption lines in stellar spectra compose an incredibly rich dataset for studies from kinematics to chemical abundances. Frequently, theoretical models predict line morphologies; we compare these predictions to observations and either validate or, more excitingly, contradict our models. If we find discrepancies between a model and a observation, we must carefully review our knowledge of the physical process that creates the observed quantity.

Fusion reactions in the cores of stars produce energy in the forms of radiation (photons) and neutrinos. Radiative energy produced in the core reaches the surface of a star after a few hundred thousand years to a few million years. As a photon crosses the outermost layers of a star, it encounters progressively cooler layers. If the photon has just the right energy, it might be absorbed by an atom or molecule, which then enters an excited state. The discrete nature of this process (i.e., that a photon must have just the right energy to be absorbed) is due to the quantum mechanical assumption that atoms can only enter discrete energy states. If the atom or molecule is unstable in this excited state, it may re-emit a photon (not necessarily of the same energy) and 'jump' down to a more stable state.

Because the photon is absorbed by the atom or molecule, we can no longer observe it. However, we can detect photons that are not absorbed; these photons eventually escape the Sun. If we take a spectrum (how the intensity varies with wavelength) of the Sun, we observe a deficiency in the number of photons at the energy required to produce the excited state of the atom. That is, we see an absorption line. Our spectrum only has information, e.g. on temperature, on the star's atmosphere – information from deeper layers, and the core, is erased by the many absorption, re-emission, and scattering processes that a photon undergos before reaching the surface of the star.

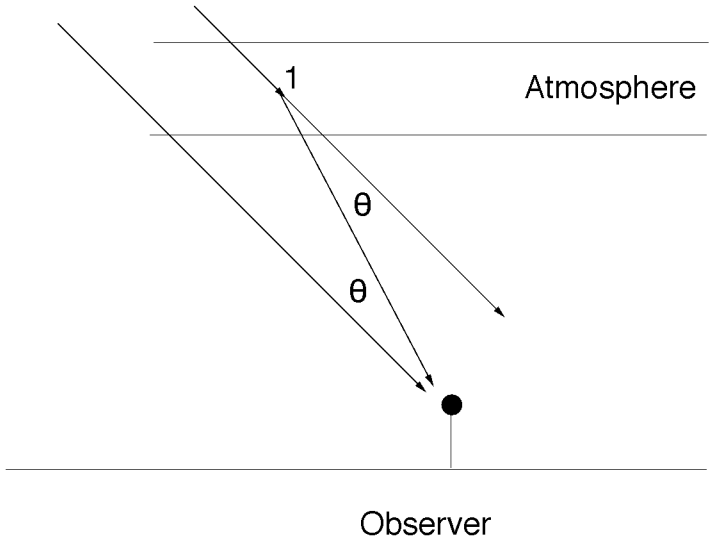

Fig. 1.— Cartoon (not drawn to scale!) of scattering in the Earth's atmosphere. We assume the Sun is far enough away that light arrives as a plane wave; if scattering happens at point 1, then simple geometry tells us that the angle between the observation and the position of the Sun is equal to the scattering angle. This geometry is only valid for a singly scattered photon.

The depth of the absorption line is an indicator of the density of absorbers in the stellar atmosphere. The Sun provides an abundance of some of the highest quality astrophysical data available, so we can detect minute differences in the depths of absorption lines. Some of these differences in depth do *not* probe the density of molecules or atoms at the solar surface; rather, these differences are due to scattering in the Earth's atmosphere (Fig. 1). As a photon of specific wavelength travels towards us, it has a chance of interacting with molecules or atoms in the Earth's atmosphere. If it does interact, its wavelength changes (except if the interaction is with aerosols), and the absorption line gets shallower (Fig. 2). It is important to recognize that scattering is fundamentally different from absorption – scattering redistributes wavelengths of photons, whereas

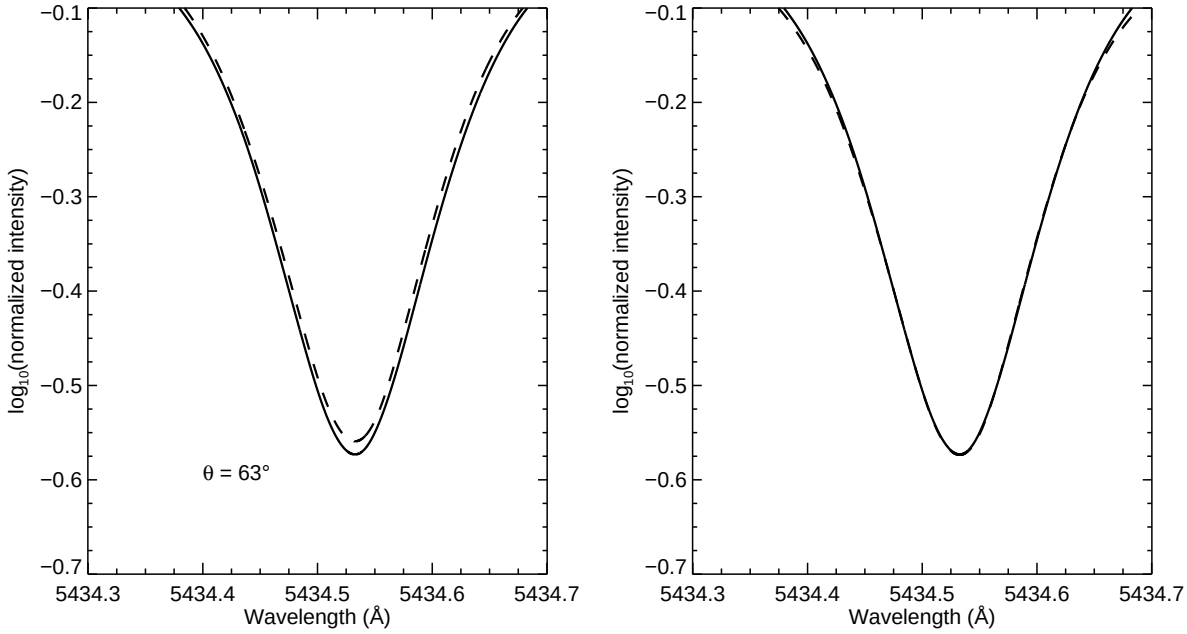

Fig. 2.— *Left*: Filling-in of an iron absorption line (dashed, $\lambda = 5434.5$) due to scattering. The reference line (solid) is convolved with the resolution of our Coudé spectrograph. *Right*: The filled-in line is corrected by 3.3%, and agrees with the reference line near the core.

absorption annihilates photons.

This paper studies the filling-in of absorption lines, a roughly 3 – 4 % effect, in order to constrain the processes that scatter light in the Earth's atmosphere. Differences in absorption line depth are evidence of the scattering process as a whole; to isolate individual scattering processes, we examine the functional dependence of line depth on angular separation from the Sun. That is, we take spectroscopic measurements of skylight at a variety of angles from the Sun and track the depth of an individual line as it varies from angle to angle. The angular distance of the measurement from the Sun is almost exactly the scattering angle, if we assume that a photon is only scattered once (Fig. 1, Gray et al. 2000). We can thus connect scattering theories that predict certain angular distributions with the observable quantity of angular separation from the Sun.

Scattering of a photon by an inelastic collision (a collision with an exchange of internal, not just kinetic, energy) with a molecule in the Earth's atmosphere is known as Rayleigh-Brillouin scattering. More specifically, Rayleigh-Brillouin scattering is due to the interaction of a photon with a sound wave, and has the form

$$f_0 = \frac{182.89 + 180.22\cos^2\theta}{191.54 + 180.89\cos^2\theta} \tag{1}$$

where θ is the scattering angle. f_0 is a factor that scales the depth of the absorption line as a function of scattering angle (Kattawar et al. 1981).

We are also concerned with aerosol scattering, or the interaction of a photon with a dust particle or liquid droplet in the Earth's atmosphere. Aerosols are much larger and more complex than molecules; Gray et al. (2000) modeled the aerosol contribution to scattering with a $\cos\theta$ term. They chose a $\cos\theta$ relation because aerosol scattering is expected to dominate at small θ; i.e., aerosols preferentially scatter light in the forward direction. This preference for forward scattering is the most important aspect to model; while aerosols can scatter light in the backwards direction, the effect is much smaller than that of the forward direction. Aerosol scattering does not change a photon's wavelength – while aerosols are larger than molecules, they are comparable in sizes to the wavelengths of visible photons. Aerosol scattering is a diffraction effect that redistributes photons in physical space, not wavelength.

A major goal of our study is to examine the contribution of ground-albedo to the filling-in of absorption lines. Ground-albedo is the reflection of light from the surface of the Earth back into the atmosphere. Several studies have examined the importance of ground-albedo (e.g., Kattawar et al. 1981), but the results are not conclusive. If ground-albedo is an important effect, the model of Gray et al. (2000) will be insufficient to explain absorption line depths; the residuals will show a systematic correlation with the positions of the Sun at the times of observation (see §3).

Gray et al. (2000) originally examined the filling-in of absorption lines as a function of angular separation from the Sun for a small set of lines around 6,000Å. Their model for line depth included Rayleigh-Brillouin and aerosol scattering:

$$d = d_0(a_0 \cos(\theta) + f_0) \tag{2}$$

where d is the line depth, θ is the angular distance of the observation from the Sun, d_0 is the average line depth across all θ, the $\cos\theta$ term is from aerosol scattering, and f_0 is from Eq. 1. They found that ground-albedo has no contribution to the filling-in of absorption lines.

The goals of this project are: to confirm the results of Gray et al. (2000) with a larger dataset of lines; to examine the wavelength dependence of scattering in the Earth's atmosphere; and, finally, to further investigate the contribution of ground-albedo to absorption line weakening. §2 details our data analysis. In §3 we show that scattering does not depend on wavelength, and that the effect due to ground-albedo must be, at best, unresolved. We examine the variation of sky brightness in the published paper (Penner & Allende Prieto 2008, in prep). In §4 we discuss the implications of our results.

2. Data analysis

We made spectroscopic observations of clear sky on 3 – 4 June 2006 using the 107" telescope at McDonald Observatory. We used the Coudé spectrograph (Tull et al. 1995) with an echelle

grating, which disperses light in two directions (i.e., a wavelength is characterized by a position (x, y) on the detector). There are 84 observations between 22° and 137° from the Sun. We show the positions of our observations in Table 1 and Fig. 3.

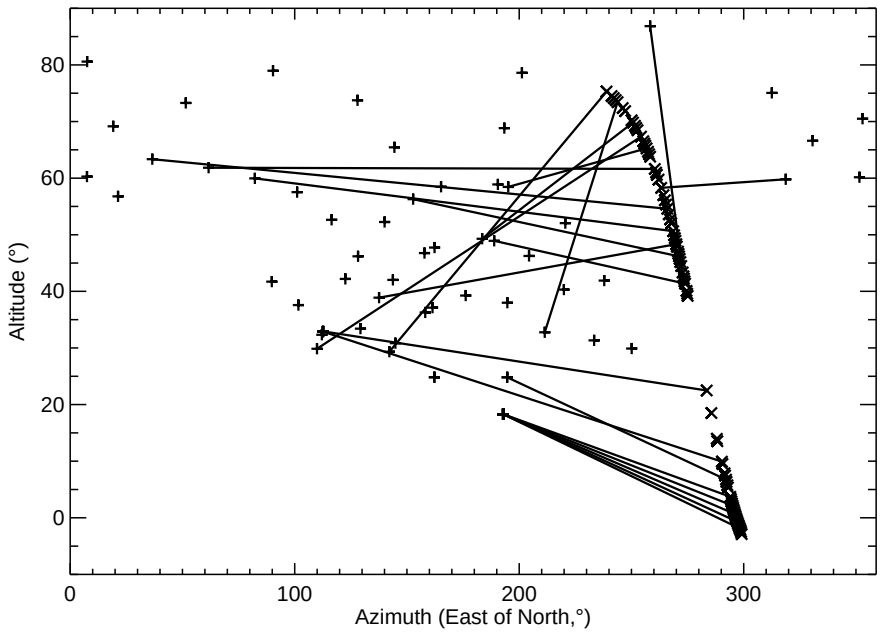

Fig. 3.— Positions of observations are shown with crosses. On the right side of the plot, marked with 'X's, are the positions of the Sun at the times of observations. For clarity, every 4th observation is connected with a line to the corresponding position of the Sun.

The Coudé spectrograph is equipped with a 1024^2 pixels Tektronix CCD. Individual frames are bias- and flat-field corrected, and scattered light (inside the detector) is modeled with polynomials and subtracted. These steps, as well as spectral extraction and wavelength calibration, are performed with IRAF[1] *echelle* tasks.

We use 103 lines from Meylan et al. (1993) that have equivalent widths $\gtrsim 50$ milli-Ångstroms. Equivalent width (EW) is the area between the absorption line and the continuum; EW is thus a measure of the strength of a line, with higher EWs corresponding to stronger lines. In lines with EW $\gtrsim 50$, noise in the continuum is a nominal effect, so a filling-in of 3 – 4% is not dominated by random fluctuations.

We use the solar atlas of Kurucz et al. (1984) for reference lines. We normalize each of the

[1]IRAF is distributed by the National Optical Astronomy Observatory, which is operated by the Association of Universities for Research in Astronomy (AURA) under cooperative agreement with the National Science Foundation.

84 spectra to the continuum; we also re-normalize the atlas spectrum to ensure a fair comparison between line depths. Our pipeline interpolates, fits, and convolves the resolution of the atlas spectrum ($\lambda/\Delta\lambda \sim 400,000$) with the modeled point spread function (approximated as a Gaussian curve) of the Coudé ($\lambda/\Delta\lambda \sim 60,000$) at the wavelength of the line being analyzed. We measure line depth by fitting splines to interpolated data and reading off the minimum flux. We measure errors by fitting a Gaussian to each line and calculating the standard deviation (σ) between the data and the Gaussian fit.

We perform a non-linear least-squares fit to Eq. 2 for each line. We use $1/\sigma^2$ weights. The two free parameters are d_0, the average line depth across many angles, and a_0, the fitting parameter we are concerned with in §3. We reject the last 6 observations because they were taken near sunset, when low signal becomes a problem (Fig. 4).

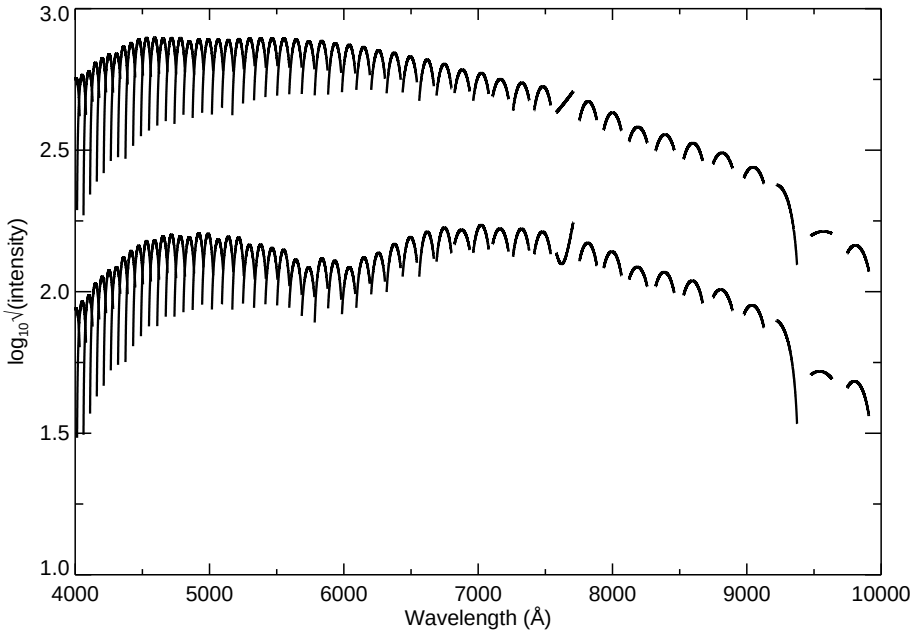

Fig. 4.— Estimated signal-to-noise ratio of two observations. If we assume Poisson statistics (photon noise), then the standard deviation $\sigma \sim \sqrt{\text{intensity}}$. The observation with lower S/N was taken near sunset. Note two aspects of this plot: one, the last observation of the day has less than half the S/N of an observation when the Sun is higher; two, the S/N in the continuum decreases in the red portion of the spectrum ($\lambda \gtrsim 7000$Å), where the instrument is inefficient. Echelle spectrographs also disperse red light over an area larger than the CCD covers, so gaps in wavelength coverage begin to appear around 7000Å. Another feature is the continuum between 7600Å and 7700Å, where oxygen in the Earth's atmosphere is a significant absorber.

3. Results

The parameters d_0 and a_0 from the least-squares fit are shown in Table 2. A few points have $a_0 < 0$; visual inspection of these lines reveals that the dependence on θ is dominated by random noise. Redder lines, specifically lines with $\lambda \gtrsim 7000$Å, show more fluctuations from the model; at least part of this is due to a decrease in the efficiency of our instrument (Fig. 4). The averaged line depths of the 103 selected lines as a function of angular separation from the Sun are shown in Fig. 5. Since we track scattering with differences in line depths (§1), we should normalize each line depth for a different θ to a chosen reference. However, for all values of θ we have the same lines, so we opt to fit the average.

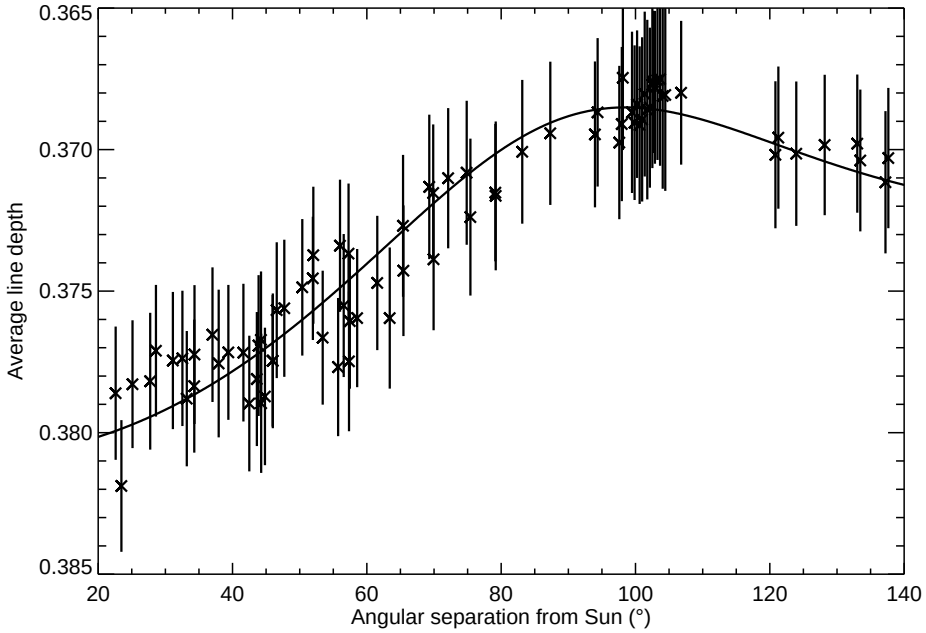

Fig. 5.— Averaged line depths of the 103 lines in Table 2 as a function of angular separation from the Sun. The solid line is Eq. 2 with parameters determined from a least-squares fit to the averaged data.

In general, the model of Gray et al. (2000) is successful in describing the functional dependence of scattering on angular separation from the Sun. If ground-albedo is an important effect, we expect the residuals to show some dependence on the altitude of the Sun, though ground-albedo may not be the only effect to correlate the two quantities. The position of the Sun in the sky determines the incident angle of light, which in turn determines the reflection angle of light. We show the residuals of the averaged line depths from the model as a function of the height of the Sun in Fig. 6. Error bars on the averaged line depths preclude us from ruling out ground-albedo as a significant contributor to the filling-in of absorption lines in the Earth's atmosphere, but we see no evolution

of the residuals with altitude of the Sun.

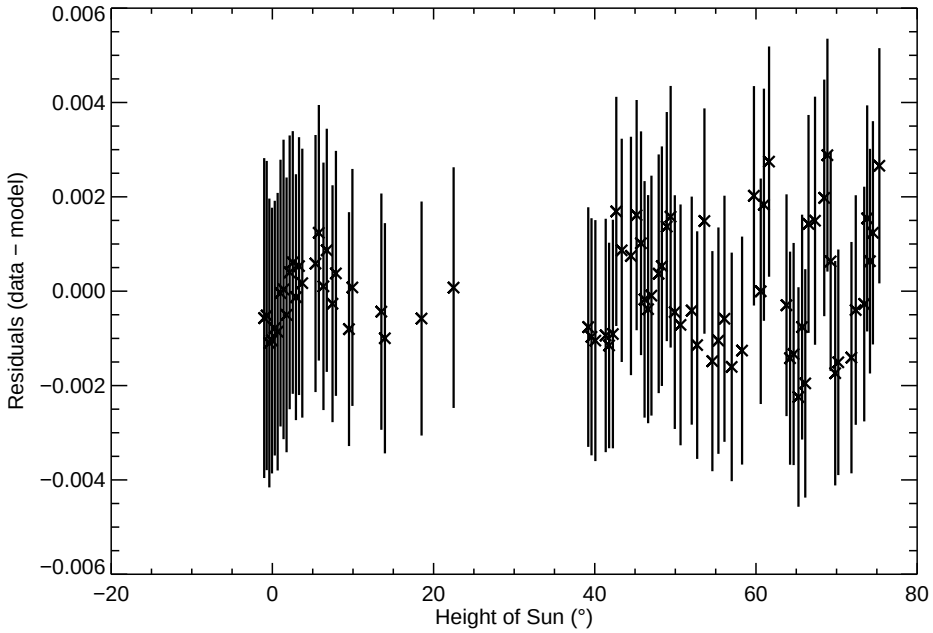

Fig. 6.— Residuals from Fig. 5 against height of the Sun. If ground-albedo is a significant effect, we expect to see a correlation of these residuals with the altitude of the Sun. We conclude that, at best, ground-albedo is an unresolved effect for this study.

Contrary to the anticipations of Gray et al. (2000), we find no dependence of the fitting parameter a_0 on wavelength (Fig. 7). The relative importance of forward and backward aerosol scattering is a function of wavelength, so Eq. 2, independent of λ, is theoretically incomplete. However, our findings suggest that the filling-in of absorption lines is not sensitive to wavelength. This result is also contrary to the simulations of Sioris & Evans (1999), though they focused exclusively on rotational Raman scattering, which we ignore.

4. Conclusion

We examine the filling-in of absorption lines to determine the dominant physical processes that scatter light in the Earth's atmosphere. The differences in absorption line depths are sufficiently modeled by Raleigh-Brillouin and aerosol scattering; ground-albedo, the reflection of light from the ground back into the atmosphere, is not an important effect. Furthermore, scattering does not depend on wavelength, although the resolution of our instrument decreases at redder wavelengths.

This work has broad implications when considering the Sun as a reference star. Studies based

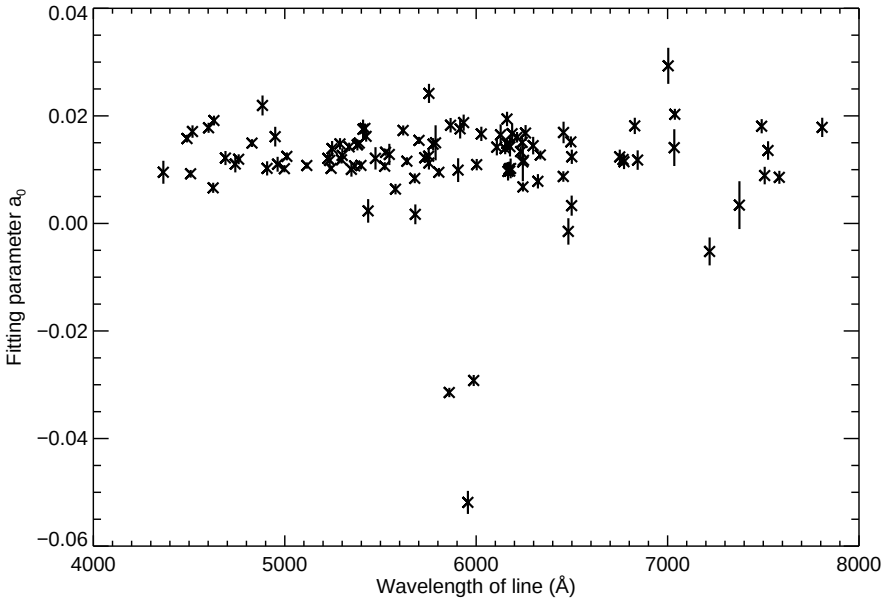

Fig. 7.— Dependence of the fitting parameter a_0 on wavelength of the absorption line. Anomalous lines with $a_0 < 0$ seem to be dominated by random noise, though the reason for this is unclear.

on ratios of line depths, or ratios of equivalent widths, or line morphologies, should not be affected by our results, since corrections for scattering obey a simple scaling law (Fig. 2). When considering absolute quantities, however, such as line depth or equivalent width alone, we must correct for any angular offset from the Sun (Gray et al. 2000).

REFERENCES

Gray, D. F., Tycner, C., & Brown, K. 2000, PASP, 112, 328

Kattawar, G. W., Young, A. T., & Humphreys, T. J. 1981, ApJ, 243, 1049

Kurucz, R. L., Furenlid, I., Brault, J., & Testerman, L. 1984, National Solar Observatory Atlas (Sunspot, NM: National Solar Observatory)

Meylan, T., Furenlid, I., Wiggs, M. S., & Kurucz, R. L. 1993, ApJS, 85, 163

Sioris, C. E., & Evans, W. F. J. 1999, Appl. Opt., 38, 2706

Tull, R. G., MacQueen, P. J., Sneden, C., & Lambert, D. L. 1995, PASP, 107, 251

This preprint was prepared with the AAS LaTeX macros v5.2.

Table 1. Observation log. Columns: 2) Universal Time of observation, 3) exposure time, 4) altitude of observation, 5) azimuth of observation, 6) altitude of Sun at observation, 7) azimuth of Sun at observation, 8) angular separation between observation and Sun.

Day	UT	T_{exp}	Alt_{obs}	Azi_{obs}	Alt_{Sun}	Azi_{Sun}	θ
	hh:ss	s	◦	◦	◦	◦	◦
Jun 3	19:48	10.0	29.34	142.14	75.31	238.93	63.41
Jun 3	19:53	10.0	36.27	158.14	74.51	241.19	53.42
Jun 3	19:55	10.0	39.25	176.16	74.15	242.11	46.00
Jun 3	19:56	10.0	38.00	194.71	73.80	242.99	42.50
Jun 3	19:58	10.0	32.76	211.38	73.43	243.86	43.88
Jun 3	20:04	10.0	31.34	233.38	72.38	246.14	41.62
Jun 3	20:06	10.0	40.31	219.91	71.85	247.19	34.34
Jun 3	20:15	10.0	46.25	204.36	70.22	250.09	32.54
Jun 3	20:17	10.0	49.28	183.51	69.83	250.72	37.02
Jun 3	20:19	10.0	47.74	162.31	69.27	251.59	45.98
Jun 3	20:21	10.0	42.03	143.75	68.87	252.17	57.34
Jun 3	20:23	10.0	33.41	129.29	68.47	252.75	69.94
Jun 3	20:29	10.0	29.86	109.93	67.33	254.28	79.19
Jun 3	20:33	10.0	42.19	122.55	66.52	255.29	65.45
Jun 3	20:35	10.0	52.26	140.03	66.12	255.79	52.04
Jun 3	20:36	10.0	58.47	165.19	65.72	256.25	39.38
Jun 3	20:39	10.0	58.44	195.13	65.27	256.76	28.60
Jun 3	20:41	10.0	52.05	220.55	64.67	257.42	22.60
Jun 3	20:44	10.0	41.90	237.90	64.23	257.89	25.11
Jun 3	20:46	10.0	29.90	250.12	63.79	258.35	34.31
Jun 3	20:56	10.0	61.83	61.65	61.63	260.44	55.72
Jun 3	20:59	10.0	73.29	51.49	60.99	261.01	44.27
Jun 3	21:01	10.0	80.59	7.56	60.59	261.37	33.19
Jun 3	21:05	10.0	75.05	312.52	59.75	262.08	23.46
Jun 3	21:12	10.0	59.79	318.74	58.28	263.28	27.74
Jun 3	21:18	10.0	66.60	330.69	56.99	264.27	31.12
Jun 3	21:22	10.0	70.49	352.94	56.09	264.93	37.94
Jun 3	21:25	10.0	69.16	19.14	55.34	265.47	46.58
Jun 3	21:29	10.0	63.34	36.58	54.59	266.00	56.01
Jun 3	21:33	10.0	56.78	21.30	53.61	266.67	57.47
Jun 3	21:38	10.0	60.28	7.46	52.71	267.27	50.39
Jun 3	21:41	10.0	60.15	351.57	52.03	267.71	44.24

Table 1—Continued

Day	UT hh:ss	T_{exp} s	Alt_{obs} ∘	Azi_{obs} ∘	Alt_{Sun} ∘	Azi_{Sun} ∘	θ ∘
Jun 3	21:47	10.0	59.96	82.26	50.64	268.60	69.30
Jun 3	21:51	10.0	57.52	101.08	49.93	269.03	72.11
Jun 3	21:53	10.0	52.64	116.42	49.41	269.35	75.42
Jun 3	21:55	10.0	46.19	128.23	48.94	269.64	79.14
Jun 3	21:58	10.0	38.89	137.57	48.33	270.00	83.14
Jun 3	22:00	10.0	30.84	144.84	47.93	270.24	87.31
Jun 3	22:04	10.0	37.12	161.39	47.03	270.76	74.87
Jun 3	22:06	10.0	46.76	157.81	46.62	271.00	69.88
Jun 3	22:08	10.0	56.28	152.76	46.18	271.26	65.39
Jun 3	22:10	10.0	65.45	144.42	45.74	271.51	61.56
Jun 3	22:13	10.0	73.75	127.97	45.19	271.82	58.56
Jun 3	22:16	10.0	78.96	90.35	44.49	272.21	56.56
Jun 3	22:21	10.0	86.85	258.31	43.35	272.83	43.62
Jun 3	22:24	10.0	78.62	201.22	42.67	273.21	44.83
Jun 3	22:26	10.0	68.83	193.36	42.25	273.44	47.71
Jun 3	22:29	10.0	58.89	190.52	41.78	273.69	51.97
Jun 3	22:30	10.0	48.93	188.87	41.36	273.91	57.27
Jun 3	22:37	10.0	41.72	89.81	40.07	274.60	98.12
Jun 3	22:39	10.0	37.57	101.66	39.59	274.85	102.62
Jun 3	22:41	10.0	32.33	112.08	39.19	275.06	106.79
Jun 3	23:59	60.0	32.94	112.63	22.49	283.55	123.94
Jun 4	00:18	60.0	32.94	112.63	18.51	285.61	128.17
Jun 4	00:41	30.0	32.89	112.58	13.96	288.04	133.02
Jun 4	00:43	30.0	32.89	112.58	13.52	288.28	133.47
Jun 4	01:01	30.0	32.89	112.58	9.93	290.29	137.21
Jun 4	01:03	30.0	32.89	112.58	9.51	290.53	137.65
Jun 4	01:11	30.0	24.82	162.21	7.88	291.49	120.83
Jun 4	01:13	30.0	24.82	162.21	7.46	291.73	121.27
Jun 4	01:17	30.0	24.81	194.66	6.75	292.16	93.96
Jun 4	01:19	30.0	24.81	194.66	6.34	292.41	94.36
Jun 4	01:22	30.0	18.31	192.84	5.76	292.76	97.59
Jun 4	01:24	30.0	18.31	192.84	5.35	293.01	97.96

Table 1—Continued

Day	UT hh:ss	T_{exp} s	Alt_{obs} ∘	Azi_{obs} ∘	Alt_{Sun} ∘	Azi_{Sun} ∘	θ ∘
Jun 4	01:32	30.0	18.31	192.84	3.71	294.04	99.49
Jun 4	01:34	30.0	18.31	192.84	3.31	294.30	99.86
Jun 4	01:37	30.0	18.31	192.84	2.92	294.56	100.24
Jun 4	01:39	30.0	18.31	192.84	2.53	294.82	100.62
Jun 4	01:41	30.0	18.31	192.84	2.14	295.08	100.99
Jun 4	01:43	30.0	18.31	192.84	1.76	295.34	101.37
Jun 4	01:45	30.0	18.31	192.84	1.38	295.60	101.75
Jun 4	01:47	30.0	18.31	192.84	1.01	295.86	102.13
Jun 4	01:49	30.0	18.31	192.84	0.65	296.13	102.51
Jun 4	01:51	30.0	18.31	192.84	0.30	296.39	102.90
Jun 4	01:53	30.0	18.31	192.84	-0.05	296.66	103.28
Jun 4	01:55	30.0	18.31	192.84	-0.38	296.93	103.66
Jun 4	01:57	30.0	18.31	192.84	-0.71	297.20	104.05
Jun 4	02:00	30.0	18.31	192.84	-1.02	297.48	104.43
Jun 4	02:02	30.0	18.31	192.84	-1.31	297.75	104.82
Jun 4	02:04	30.0	18.31	192.84	-1.60	298.02	105.20
Jun 4	02:06	30.0	18.31	192.84	-1.89	298.30	105.59
Jun 4	02:08	30.0	18.31	192.84	-2.18	298.58	105.98
Jun 4	02:10	30.0	18.31	192.84	-2.49	298.86	106.36
Jun 4	02:12	30.0	18.31	192.84	-2.88	299.14	106.75

Table 2. Model parameters for Eq. 2

λ of line (Å)	d_0	a_0
4365.90	0.44	0.0095 ± 0.0021
4489.75	0.67	0.0158 ± 0.0007
4508.28	0.58	0.0092 ± 0.0007
4518.03	0.54	0.0171 ± 0.0012
4602.01	0.54	0.0178 ± 0.0009
4626.19	0.59	0.0066 ± 0.0009
4630.12	0.51	0.0191 ± 0.0009
4690.14	0.41	0.0122 ± 0.0013
4741.55	0.52	0.0110 ± 0.0015
4759.28	0.35	0.0119 ± 0.0009
4829.03	0.51	0.0149 ± 0.0007
4883.70	0.43	0.0219 ± 0.0019
4907.73	0.43	0.0102 ± 0.0013
4950.12	0.49	0.0161 ± 0.0018
4962.57	0.37	0.0110 ± 0.0014
4998.24	0.39	0.0102 ± 0.0007
5010.95	0.35	0.0125 ± 0.0007
5115.40	0.48	0.0108 ± 0.0006
5225.53	0.49	0.0121 ± 0.0008
5234.63	0.52	0.0117 ± 0.0017
5242.50	0.54	0.0102 ± 0.0005
5247.58	0.53	0.0139 ± 0.0014
5288.53	0.38	0.0148 ± 0.0011
5296.70	0.58	0.0119 ± 0.0007
5300.76	0.41	0.0126 ± 0.0013
5336.79	0.45	0.0142 ± 0.0008
5348.32	0.58	0.0100 ± 0.0014
5365.41	0.48	0.0107 ± 0.0008
5379.58	0.40	0.0146 ± 0.0010
5381.03	0.38	0.0147 ± 0.0005
5389.49	0.50	0.0149 ± 0.0006
5398.29	0.44	0.0108 ± 0.0008
5409.15	0.35	0.0175 ± 0.0018

Table 2—Continued

λ of line (Å)	d_0	a_0
5418.78	0.33	0.0177 ± 0.0009
5425.26	0.25	0.0162 ± 0.0010
5435.87	0.34	0.0023 ± 0.0022
5473.91	0.47	0.0121 ± 0.0021
5522.46	0.28	0.0106 ± 0.0007
5526.82	0.46	0.0132 ± 0.0006
5546.51	0.32	0.0128 ± 0.0020
5578.73	0.36	0.0064 ± 0.0010
5618.64	0.31	0.0173 ± 0.0009
5638.27	0.45	0.0116 ± 0.0007
5679.03	0.36	0.0084 ± 0.0009
5682.23	0.32	0.0017 ± 0.0018
5701.55	0.48	0.0154 ± 0.0007
5731.77	0.35	0.0122 ± 0.0010
5752.04	0.34	0.0125 ± 0.0013
5753.13	0.45	0.0112 ± 0.0012
5753.66	0.22	0.0242 ± 0.0018
5775.09	0.36	0.0147 ± 0.0011
5787.92	0.28	0.0150 ± 0.0033
5805.21	0.25	0.0095 ± 0.0008
5859.61	0.46	-0.0314 ± 0.0009
5866.47	0.30	0.0183 ± 0.0013
5905.67	0.34	0.0099 ± 0.0022
5916.25	0.33	0.0176 ± 0.0018
5934.67	0.42	0.0187 ± 0.0015
5956.71	0.38	-0.0519 ± 0.0021
5987.05	0.41	-0.0292 ± 0.0010
6003.01	0.44	0.0109 ± 0.0011
6027.05	0.37	0.0167 ± 0.0013
6108.12	0.38	0.0142 ± 0.0015
6127.91	0.29	0.0165 ± 0.0019
6151.62	0.31	0.0139 ± 0.0011
6160.75	0.30	0.0149 ± 0.0009

Table 2—Continued

λ of line (Å)	d_0	a_0
6161.30	0.34	0.0194 ± 0.0013
6166.46	0.40	0.0097 ± 0.0017
6173.36	0.41	0.0102 ± 0.0013
6175.39	0.30	0.0097 ± 0.0007
6176.82	0.36	0.0143 ± 0.0018
6180.23	0.33	0.0102 ± 0.0018
6188.01	0.28	0.0167 ± 0.0019
6213.43	0.45	0.0160 ± 0.0010
6232.64	0.45	0.0134 ± 0.0010
6240.65	0.29	0.0151 ± 0.0008
6243.81	0.23	0.0114 ± 0.0036
6244.47	0.24	0.0068 ± 0.0009
6247.55	0.29	0.0117 ± 0.0010
6258.11	0.31	0.0168 ± 0.0015
6297.82	0.43	0.0145 ± 0.0016
6322.68	0.41	0.0078 ± 0.0013
6335.33	0.50	0.0127 ± 0.0008
6455.60	0.31	0.0087 ± 0.0010
6456.39	0.33	0.0169 ± 0.0020
6481.87	0.36	-0.0015 ± 0.0025
6494.99	0.62	0.0152 ± 0.0010
6498.95	0.28	0.0033 ± 0.0019
6499.66	0.46	0.0124 ± 0.0013
6750.15	0.40	0.0124 ± 0.0014
6767.79	0.43	0.0119 ± 0.0011
6772.34	0.27	0.0115 ± 0.0014
6828.59	0.28	0.0181 ± 0.0015
6843.66	0.31	0.0118 ± 0.0018
7003.57	0.25	0.0293 ± 0.0033
7034.92	0.28	0.0141 ± 0.0034
7038.24	0.30	0.0203 ± 0.0010
7219.70	0.25	-0.0052 ± 0.0026
7375.27	0.13	0.0034 ± 0.0044

Table 2—Continued

λ of line (Å)	d_0	a_0
7491.65	0.31	0.0181 ± 0.0013
7507.29	0.29	0.0089 ± 0.0016
7525.14	0.34	0.0136 ± 0.0017
7583.79	0.38	0.0086 ± 0.0012
7807.91	0.26	0.0179 ± 0.0018
Average	0.39	0.0111 ± 0.0015